RSC Advances

ROYAL SOCIETY OF CHEMISTRY

www.rsc.org/advances

RSC Advances

ARTICLE

Optimization of PEG Coated Nanoscale Gold Particles for Enhanced Radiation Therapy

C. Cruje,[a] C. Yang,[a] J. Uertz, [b] M. van Prooijen, [c] and B. D. Chithrani[a,d]

Received 00th January 20xx,
Accepted 00th January 20xx

DOI: 10.1039/x0xx00000x

www.rsc.org/

Nanoscale gold particles are being used as a radiation dose enhancer in cancer research. The purpose of this study was to optimize the uptake of Polyethylene Glycol (PEG) functionalized gold nanoparticles (GNPs) for an enhanced therapeutic effect during radiation therapy. PEG is widely used in providing NPs with stealth properties, thus prolonging blood circulation times. However, PEG minimizes PEG-GNP interaction with cell surface ligands resulting in significantly lower in *vitro* cellular uptake. As intracellular localization of GNPs maximizes its therapeutic enhancement, there is a need to improve the uptake of PEG-GNPs. To enhance uptake, RGD peptide containing an integrin binding domain was conjugated along with PEG. Spherical GNPs of diameters 14 and 50 nm and PEG chain lengths of 2 kDa were used for the study. Nanoparticles functionalized with both RGD peptide and PEG had higher uptake than NPs functionalized with PEG alone. The enhancement in uptake was higher for 14 nm NPs as compared to 50 nm NPs. Our radiation therapy results showed that smaller NPs conjugated with PEG and RGD peptides have a three-fold therapeutic enhancement as compared to larger NPs in MDA-MB-231 cells at clinically relevant 6 MV energy. This study will shed light on clinical use of GNPs in radiation therapy in the near future.

1. Introduction

The biomedical research of inorganic nanoparticles (NPs) has developed NP-based cancer therapeutics and imaging[1-3]. Through such applications, disease may be managed safely and more efficiently[4]. NP platforms are being developed to target therapeutics to tumors while minimizing interaction with normal tissue [5]. To achieve an efficient NP system, prolonged *in vivo* residency time, preferential localization in tumor environments, and cancer cell internalization for applications that favor intracellular localization is required [6-8]. Longer blood circulation time is important because NPs should not be cleared from the body before interaction with tumor tissue. To achieve favorable blood circulation times and cancer cell targeting, various NP sizes, shapes and surfaces have been studied [9-12]. Colloidal gold NPs (GNPs) whose surface was modified with folic acid, were found to deliver doxorubicin more effectively to HeLa cells in comparison to healthy (MDCK) cells [13]. Similarly, magnetic iron oxide NPs that targeted urokinase plasminogen activator receptors were found to be effective for drug delivery and imaging of cells that overexpressed such receptors [14]. Peptides containing the arginine-glycine-aspartic acid (RGD) sequence have been receiving extensive attention recently because they can recognize the integrin αvβ3 that is highly expressed by several solid tumors[3, 15]. It is important to prolong blood circulation times since tumor uptake of NP's is slow. Prolonged blood circulation time of NPs is achieved by surface modification of NPs with Polyethylene Glycol (PEG) or PEGylation, as found in numerous *in vivo* studies[1, 4, 6, 16, 17]. For example, Lipka *et al* showed that a longer PEG chain length of 10kDa improved NP blood circulation time, with over 15% of applied volume still circulating in the bloodstream of mice subjects 24 hours after injection [17].

NPs functionalized with PEG have the capability to evade uptake by macrophage cells in the immune system, achieving longer blood circulation times. One of the proteins in the blood that the NP surface should be protected from is opsonin [18, 19]. As illustrated in **Figure 1A** opsonin protein can bind to the surface of the as made GNPs. These opsonin bound NPs will be removed from the blood by macrophage cells in the blood (see the left side of **Figure 1B**). Hence, as made GNPs clears from the body within an hour of intravenous application[17-19]. It was found that a minimum density of 1 PEG/nm^2 is required to achieve a significant reduction in nonspecific protein adsorption in the blood [19, 20]. PEGylation of NPs allows for a higher likelihood of NP entry and retention in tumor tissue. Tumor blood vessels have leaky capillaries allowing NPs to leak into tumor tissue as shown in Figure 1B [7, 21]. Hence, the longer circulation period allows for a higher chance of preferential accumulation of NPs in the tumor tissue [22]. For example, PEG-coated liposomes sized 100-200 nm are being currently used as delivery vehicles for FDA-approved chemotherapeutic drugs such as doxorubicin and oncospar [22]. However, recent studies using inorganic NPs, such as colloidal GNPs, showed lower uptake when functionalized with PEG, as discussed in the next section.

PEG-coated GNPs are found to have decreased cellular uptake *in vitro* and *in vivo* [18, 23-25]. Nativo *et al.* found that PEG-coated GNPs

[a] Dept. of Physics, Ryerson University, Toronto, ON, M5B 2K3, Canada; Email: devika.chithrani@ryerson.ca.
[b] CytoViva Inc., 570 Devall Drive, Auburn, AL, 36832, USA.
[c] Princess Margaret Cancer Centre, Toronto, ON, M5G 2M9.
[d] Keenan Research Centre, Li Ka Shing Knowledge Institute, St. Michael's Hospital, Toronto, ON, M5B 1W8, Canada.

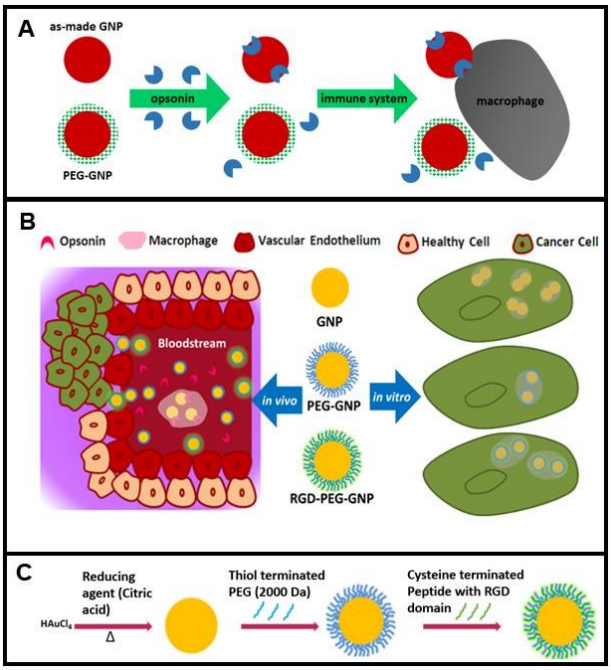

Fig. 1. (A) PEG molecules are used to screen NPs against opsonin protein found in the blood. Opsonin marks NPs for macrophage detection which is then followed by their clearance from the body through macrophages. (B) Ideal NP design for maximum tumor cell accumulation. Prolonged lifetime of NPs in the bloodstream is foremost to its design as such will take advantage of the EPR effect in tumor environments. PEGylation improves the residency time in the blood, but decreases the NPs at a single cell level. Combination of PEG and a peptide (RGD) containing integrin binding domain could improve the NP accumulation at single tumor cell level both *in vitro* (left side) and *in vivo* (right side). (C) Preparation of NPs for the study. Gold salt solution was brought to boil and added the reducing agent to form NPs. For functionalization, NPs were mixed with PEG first followed by addition of peptide containing RGD domain.

had significantly less uptake by HeLa cells [23]. Similarly, Arnida *et al.* found the same trend using PC-3 cells [18]. These studies suggest that PEG-coated GNPs localize external to cancer cells in interstitial tissue. Chemotherapeutic toxicity relies on the entry of drugs into cancer cells [24, 25]. NP cellular uptake was also found to correlate with the sensitization of cancer cells to radiation therapy [26, 27]. To improve the cellular internalization of PEG-coated NPs, previous studies explored functionalization with endocytosis-enhancing ligands, such as Herceptin and peptides [28, 29]. For example, Liu *et al.* showed that RME-peptide functionalized PEG-coated GNPs with a core diameter of 10 nm had an enhanced uptake in HeLa cells *in vitro* in comparison to GNPs coated with PEG alone [29]. These promising findings imply that an understanding of cell-targeting PEG-coated NPs is necessary in order to move forward with NP-based medical treatments such as chemotherapy and radiation therapy. However, we still do not know how the size of the NPs affect their uptake and resulting therapeutic effect when NPs are functionalized with PEG and special peptides (to improve cell uptake).

Our previous studies showed that the uptake of colloidal GNPs was size dependent and GNPs of size 50 nm showed the highest uptake among the size range 14-100 nm [30]. We also showed that radiation dose enhancement properties of colloidal GNPs was size dependent [26]. For example, 50 nm size GNPs were more effective than 14 nm sized GNPs. However, these GNPs were not functionalized with PEG. As we discussed before, PEG can minimize the GNP uptake at a single cell level (see the right side of Figure 1B). Hence, the goal of this study was to use a peptide containing integrin binding domain, RGD, in combination with PEG to improve the NP uptake and to investigate the change in cell uptake and radiation therapy response as a function of the size of colloidal GNPs. The schematic Figure 1C illustrates the preparation of NPs for this study.

2. Experimental

2.1. GNP synthesis and characterization

The citrate reduction method was used to synthesize GNPs of diameters 14 and 50 nm. 300 mL of 1% $HAuCl_4 \bullet 3H_2O$ was added to 30 mL of distilled water and was brought to a boil while continuously stirring. At boiling point, 600 and 113 µL of 1% anhydrous citric acid was added to synthesize small and medium sized GNPs respectively. For small GNPs, the color of the solution changed from dark blue to red. However, for medium sized GNPs, the color of the solution changed from black to maroon. After no further color change was observed, all solutions were left to boil for another five minutes. GNP solutions were then brought to room temperature while stirring, then refrigerated. GNPs were characterized with UV-visible spectrophotometry, Dynamic Light Scattering (DLS), Zeta potential measurements, and Transmission Electron Microscopy (TEM).

2.2. PEGylation of GNPs

We used PEG of molecular weight 2000 Da since our preliminary data showed very low NP uptake when PEG of molecular weight 5000 Da was used[31]. A 1% PEG solution was prepared with thiol-terminated PEG methyl ether of molecular weight 2000 Da. The solution was added to GNP solutions to achieve a grafting density of 1 PEG molecule per nm^2. For 14 and 50 nm GNPs, 616 and 7854 PEG molecules were added per NP. To confirm PEGylation of GNPs, DLS measurements were conducted. This was followed by UV-visible spectrophotometry to confirm stability.

2.3. Peptide-functionalization of PEG-GNP

Following PEGylation of GNPs, the peptide sequence CKKKKKKGGRGDMFG was added to solutions to ensure that the number of RGD peptides matched that of PEG molecules. This peptide containing RGD domain was used since it is molecular weight was closer to the PEG we used for the experiment. For all conjugates, UV-visible spectrophotometry and DLS were done to confirm minimal shift in size and that no aggregation occurs.

2.4. Cellular uptake study

MDA-MB-231 cells were cultured in Dulbecco's Modified Eagle's Medium with 10% Fetal Bovine Serum grown to confluent so that three wells of a 6-well tissue culture dishes were incubated with the same NP type. For optical imaging purposes, MDA-MB-231 cells were placed on glass coverslips and grown to 60% confluent. Cell cultures were incubated with $5x10^{10}$ GNPs per dish for fourteen hours. Following incubation, all cell cultures were washed with Phosphate-Buffered Saline (PBS) three times. Those without coverslips were trypsinized and processed for quantification described in the next section. Those with coverslips were rinsed twice with PBS, followed by fixation with 4% paraformaldehyde in PBS for 10 minutes at room temperature, then rehydration in PBS. Coverslips were mounted onto glass slides and were dried overnight for microscopy.

2.5. GNP uptake quantification

Harvested cells were counted prior to processing for Inductively Coupled Plasma Atomic Emission Spectroscopy (ICP-AES). To prepare samples for ICP-AES, HNO_3 was added to samples that were boiled at 200°C in an oil bath for cell digestion and GNP atomization. ICP-AES of samples was then performed and resulting gold atom counts were converted to GNPs per cell.

2.6. Visual evaluation by CytoViva microscopy

To qualitatively confirm quantification results from ICP-AES, CytoViva microscopy of cells was done. This imaging system was designed so that despite NP interaction with cells or tissue, their spectra may still be confirmed because they are still optically observable. The microscope is a dark-field imaging system that uses oblique angle lighting. The result is high signal-to-noise optimized dark-field based images. NPs appear bright due to high scattering cross-sections of GNPs. To confirm the spectra of GNPs, SAM (Spectral Angle Mapping) was conducted with the CytoViva hyperspectral imaging system. SAM determines the presence of GNPs in the input image by comparing unknown spectra in the acquired hyperspectral image to a user-defined spectrum, which is that of a GNP in these experiments.

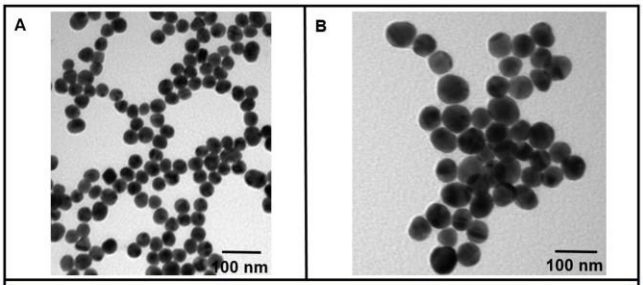

C Surface Ligand	Hydrodynamic Diameter		Peak Wavelength (nm)	
Size of GNPs (nm)	14	50	14	50
Citrate	14.7 ± 1.7	53.5 ± 1.3	518	532
PEG	18.6 ± 1.3	58.4 ± 1.4	519	533
PEG/RGD	18.8 ± 1.5	59.1 ± 1.6	519	533

Fig. 2. Characterization of GNPs. (A-B) Transmission Electron Microscopy images of colloidal GNPs of diameter 14 and 50 nm. (C) UV-Visible Spectroscopy and Dynamic Light Scattering data for as made (citrate coated), PEG-coated, and PEG/RGD coated GNPs.

2.7. Radiation and GNP treatment

MDA-MB-231 cells were incubated with varying NPs followed by a single radiation fraction treatment using a megavoltage photon beam (6 MeV). Here, 6-well dishes were used and $1x10^{10}$ GNPs were added per dish. An Elekta Synergy linear accelerator (Elekta Oncology Systems, Stockholm, Sweden) was used as a 6 MeV photon source. Plastic bolus 2 cm thick, like the dishes used, was cut out so that dishes were surrounded by water equivalent material in lieu of air. 10 cm of solid water was placed under the dish for backscatter while 8 cm was placed above it. The monolayer was then set-up to a source-to-axis distance of 100 cm. A field size of 40 cm x 40 cm was used so that all the wells were irradiated with 2 Gy at a dose rate of 600 MU/min at the same time. The survival fraction of irradiated samples were compared to non-irradiated and no NP samples. This experiment was repeated three times.

2.8. Survival fractions of irradiated cells

A clonogenic assay was performed for all treatment conditions. 10 cm dishes were seeded with 100 cells from the non-irradiated samples or 200 cells from the irradiated cultures. Three dishes were prepared per sample type. After two weeks of seeding, the number of colonies per dish were counted and compared to that of the control.

2. Results

3.1. Characterization and biocompatibility of NPs

GNPs of diameter 14 and 50 nm were characterized using TEM, DLS and UV Visible Spectroscopy (as shown in **Figure 2**). According to TEM images, the average size of the 14 and 50 NPs were about 13.8 and 48.2 nm, respectively. The TEM images of GNPs modified with PEG/RGD combination were given in supplementary section **S1**. The surface plasmon resonance (SPR) has been observed for as made, PEG-coated, and PEG-RGD coated gold NPs using optical absorption, and the values are listed in **Figure 2**. A small red shift in the SPR peak wavelength was seen for NPs conjugated with PEG and RGD peptides. This is closely related to the increase in size of the NPs due to PEG and RGD molecules on the NP surface as explained by Mie theory. Dynamic light scattering measurements also showed an increase in size for PEG and PEG/RGD conjugated NPs. Based on zeta potential measurements, the z potentials of 14 and 50 nm as made gold particles were -18.23, and -10.27 mV, respectively, and these high z potentials are due to citric acid coating and negative charge on the surface. The PEG coating induces the decreases of z potentials to -4.55 (±0.57) and -2.07 (±0.45) mV, respectively. The PEG/RGD

coating further reduced the negative surface charge to -2.55 (±0.65) and -1.065 (±0.53) mV, respectively

The biocompatibility of NPs was assessed using DNA DSBs assay, clonogenic assay and confluence assay. As illustrated in **Figure 3**, these NPs did not cause any cytotoxicity at concentrations used in this study. For example, the clonogenic assay showed no significant difference in cell survival due to the presence of NPs. This was a long term assay where we monitored the growth for two weeks. We also monitored the growth of cells in short term (for 48 hours) to investigate whether there is an effect on cell division due to the presence of NPs. There was no significant difference in cell growth in the presence of NPs. DNA DSBs assay showed no enhancement in the

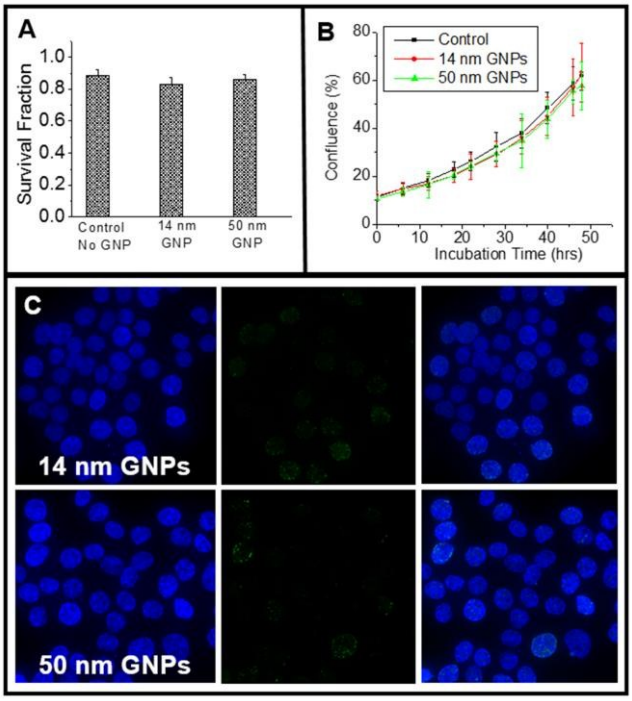

Fig. 3. Biocompatibility of GNPs used for the study. (A) Cell survival fraction was monitored using clonogenic assay. (B) Variation of cell growth or cell proliferation was monitored with IncuCyte™ Kinetic Live Cell Imaging System with a 2-hour time interval for 48 hours. (C) DNA double strand break assay was performed for monitoring the toxicity introduced by GNPs. The cell nucleus is shown in blue while the repair protein 53BP1 is marked in green.

DNA damage due to the presence of NPs. This is in agreement with our previous studies[32]. We have shown the cell survival data and confluency assay of GNPs functionalized with PEG and PEG/RGD in supplementary section **S2**.

3.2. Cellular uptake of as made, PEG-coated, and PEG-RGD-coated GNPs

Our recent study showed that smaller NPs (size 20 nm) penetrate better in tumor tissue compared to larger NPs (50 and 74 nm) [33]. However, NPs should be PEGylated for their delivery to tumor tissue. Hence, in this study, we used 14 and 50 nm GNPs to investigate the effect of RGD peptide on the uptake of PEG-coated NPs (see **Figure 4**). In contrast to results of the previous study, 50 nm diameter GNPs had a higher uptake as compared to 14 nm GNPs. Once PEGylated, both NP sizes had a lower cell uptake (as illustrated in **Figure 4)**. Th introduction of the RGD peptide enhanced the uptake of smaller NPs, but not the larger ones. The smaller NPs conjugated with PEG and RGD showed three-fold increase in uptake as compared to PE coated NPs. We have also tested GNPs of size 74 nm and results were similar to 50 nm GNPs (see the supplementary section **S3**). This clearly shows that smaller NP are better compared to larger NPs since they have a higher probability of internalization with the help of the peptide containing integrin binding domain. We believe that the higher curvature of small NPs opens up space for RGD peptide to access the surface receptors on the cell membrane while these

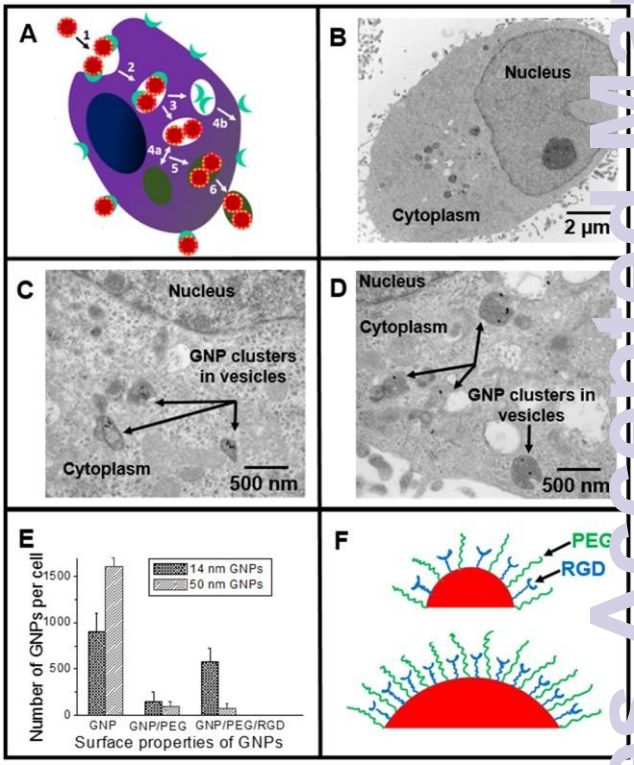

Fig. 4. Cellular uptake of GNPs. (A) The RME process of GNP entry into cells GNPs nonspecifically adsorb serum protein, which facilitate RME. Th events are as follows as labelled above. 1 – interaction with cell membrane receptor, 2 – endocytosis, 3 – sorting, 4a – fusion with lysosome, 4b recycling of receptors, 5 – transport to cell membrane, 6 – exocytosis. (B) Cross sectional TEM image of a cell. (C-D) Cross-sectional TEM image showing GNPs of size 14 and 50 nm localized in small vesicles of the cell respectively. (E) Quantification of NP uptake per cell. It was possible t enhance the uptake of PEG coated GNPs using the RGD peptide. (F) Schematic showing the higher accessibility of RGD peptide with the high surface curvature of smaller NPs.

peptides can be hidden between PEG molecules in larger NPs due to lower surface curvature as explained in the schematic in **Figure 4**. The ability to access the surface receptors of cancer cells led to an increase in uptake of smaller NPs. This would be very important for therapeutic applications, such as radiation therapy and drug delivery applications. In the next section, we will discuss the use of GNPs for radiation therapy at clinically relevant MeV energies.

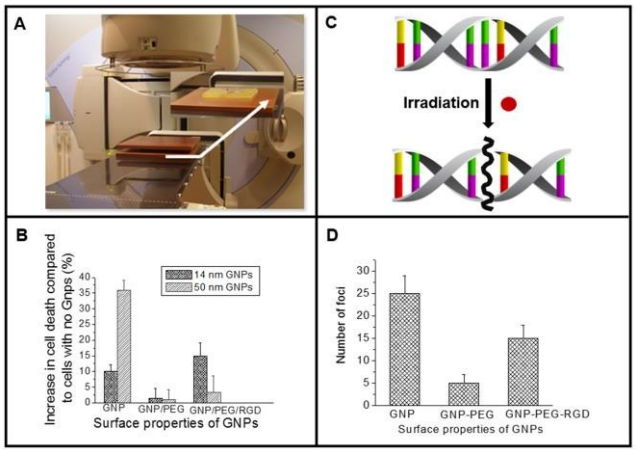

Fig. 5. Quantitative assessment of effect of radiation treatment on MDA-MB231 breast cancer cell line using 6 MV X rays. (A) Experimental set up of the linear accelerator used for the treatment of the cells. (B) Enhancement in cell death as compared to cells with no GNPs after a radiation dose of 2 Gy. (C) Schematic showing the increased probability of DNA DSBs in the presence of GNPs during a radiation treatment. (D) Quantification of 53BP1 radiation-induced foci after 2 Gy 6 MV X-ray photons [cells pre-treated with gold nanoparticles].

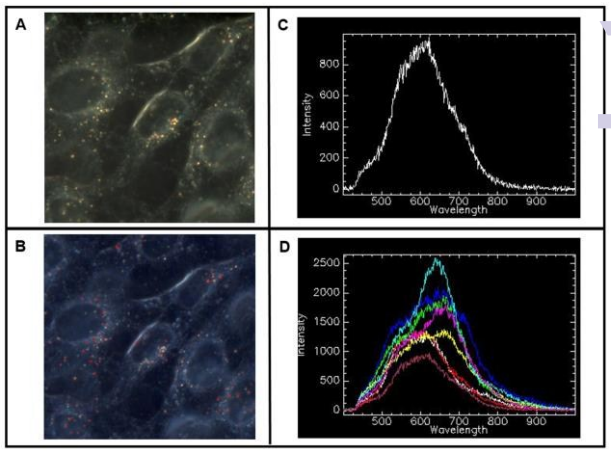

Fig. 6. CytoViva hyperspectral imaging of GNPs (size-14 nm, GN functionalized with PEG/RGD) internalized in cells. (A) The dark field image of GNPs in cells. (B) The spectral angle map overlaid onto tl hyperspectral dark field image. The spectrum from each pixel is compared to a reference reflectance spectra (panel C) from gold and if a match is determined, the pixels are colored red. (D) Reflectance spectra from few GNP clusters localized within cell shown in (A).

3.3. Radiation sensitization due to NPs was dependent on size and surface properties

Our study has shown that radiation sensitization due to as made GNPs was dependent on size and surface properties at clinically relevant MeV energies (see **Figure 5**). For example, as made (or citrate capped) NPs of size 14 nm had lower sensitization at clinically relevant energies as compared to larger NPs of size 50 nm. This is due to the fact that smaller NPs have lower uptake as compared to larger NPs. It is important to PEGylate NPs for their use *in vivo*. However, PEGylated NPs of both sizes had insignificant sensitization effects since their uptake is very low as shown in **Figure 4**. As discussed in the previous section, we were able to improve the uptake of smaller NPs using a peptide containing integrin binding domain. This resulted in an increase in cell death due to radiation dose enhancement at clinically relevant MeV energies only for smaller NPs as shown in **Figure 5**. This is the first time that it was shown that smaller NPs can be used as a radiation dose enhancer at clinically relevant energies with the use of a peptide containing integrin binding domain. We used clonogenic assay to measure the effect of radiation dose enhancement during the radiation treatment at MeV energies.

3.4. Mapping of GNP distribution using CytoViva technology

The CytoViva technology was specifically designed for optical observation and spectral confirmation of NPs as they interact with cells and tissues. **Figure 6A** is a dark field image of a group of cells with internalized GNPs. The GNPs appear bright, owing to their high scattering cross-section. With the integrated CytoViva hyperspectral imaging capability, reflectance spectra from specific materials can be captured and measured. **Figure 6B** shows few reflectance spectra from GNPs. SAM (Spectral Angle Mapping) is an automated procedure used to determine if GNPs are present in the input image, and it locates the pixels that contain the material of interest. SAM accomplishes these tasks by comparing unknown spectra in the hyperspectral image with known spectra for the material of interest. In this situation, the materials of interest are GNPs. The hyperspectral image shows the relative degree to which the unknown spectra in each image pixel matches the known GNP spectrum. **Figure 6C** shows the hyperspectral image with an overlaid spectral angle map with the red dots representing GNP clusters mapped to the reference spectra shown in **Figure 6D**.

Figure 6 is a two dimensional mapping (XY plane) of NP distributi within cells. The most interesting feature of this technology is that it is not necessary to optically label NPs since optical scattering by NPs are being used for imaging. GNPs are very good scatters of light ir the visible region. In addition, this imaging technology allows us to

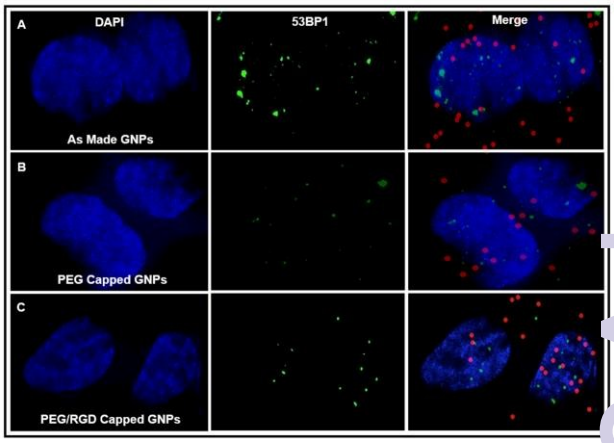

Fig. 7. 3D projection of GNP clusters and DNA DSBs for cells treated wi 2 Gy radiation dose. Three panels represent images of cells internalized wi as made GNPs (panel A), PEG coated GNPs (panel B), and PEG/RGD coated GNPs (panel C).

verify imaged NP clusters within cells by looking into their reflectance spectra as illustrated in **Figure 6**. GNPs have a unique reflectance spectra peaked between 550 and 650 nm. The areas where no NP are seen, the reflectance spectra appears very broad and flat as shown supplementary section S3. The small bright dots are GNP clusters localized within cells. As illustrated in the supplementary section **S4**, two-dimensional cross sectional view of a cell (both optical and TEM images) clearly shows the nucleus (with no GNPs) and the NP clusters localized within small vesicles within the cytoplasm. However, it was just a two-dimensional view. Distribution of NPs in selected different planes of the cells is shown in supplementary section **S5**. It clearly showed that most of the NP clusters were localized within the cell. It is impossible to obtain such a three dimensional (3D) distribution of NPs using TEM. Using the hyperspectral imaging technique, we were able to map the 3D distribution of NPs and DNA DSBs simultaneously for the first time. In this case, dark field images were taken along the Z-direction (~ 55 slices) and the data was deconvoluted for clarity. **Figure 7** shows the 3D NP distribution projected onto a single plane since it is difficult to show all 55 images taken across the cell. The red dots are NP clusters localized within cells. The blue areas are nuclei of cells. We were able to show that our NP quantification data correlates with our optical imaging data. For example, more NPs were seen in cells incubated with as made or PEG/RGD GNPs as compared to PEG coated GNPs. Our next goal was to look into how the NP distribution relates to DNA DSBs during a radiation experiment and we mapped the DNA DSBs along with the NP distribution to address this issue.

3.5. Assessment of the Enhancement of DNA DSBs in Cells

A direct correlation between DNA DSBs and cell survival *in vitro* had been discovered[34]. However, we still do not know the direct correlation between NP distribution and DNA DSBs. The experimental setup for the irradiations is shown in the top left panel of **Figure 4**. To quantify the DSBs, a minimum of 50 nuclei from each sample were assayed using image intensity-based thresholding and segmentation. The protein 53BP1 that is present at the sites of DNA DSBs was probed using wide-field imaging. The results are shown in **Figures 4B and 7**. We used smaller NPs to show correlation with DNA DSBs and number of NPs localized. The top, middle, and bottom panels in **Figure 7** show images corresponding to cells with citrate capped GNPs, PEG-coated, and PEG-RGD coated GNPs, respectively. These images correspond to nuclei of cells that were irradiated and fixed 24 hrs later. According to our quantification and qualitative data, citrate capped NPs have more NPs per cell and the highest number of DNA DSBs. The most interesting result is the mapping of both DNA DSBs and GNPs. We saw more DNA DSBs in cells internalized with more NPs. So far we have seen this outcome only quantitatively[26]. We were able to map simultaneously the internalized NP clusters and DNA DSBs for the first time and showed that more DNA DSBs can be seen for cells internalized with more NPs after a radiation treatment at clinically relevant MeV energies. For example, cells targeted with GNPs modified with PEG/RGD had a higher uptake leading to more DNA DSBs during a radiation treatment as compared to untargeted PEGylated GNPs. Hence our data support enhanced sensitization by targeted NPs over untargeted However, we are still not able to correlate location of GNP clusters to DNA DSBs. We will study this in our future studies.

Discussion

The emerging field of nanomedicine requires better understanding of the interface between nanotechnology and medicine. Better knowledge of the nano-bio interface will lead to better tools for diagnostic imaging and therapy. Gold nanostructures are used as a model system in this regard since their physical and chemical properties can be easily manipulated. In the size range of 10-100 nm, GNPs of diameter 50 nm have the highest uptake compared to smaller and larger NPs[30]. These NPs mostly enter the cell *via* receptor mediated endocytosis (RME) as explained in the schematic **Figure 4A**. This involves the binding of the NPs to cell membrane receptors followed by membrane wrapping for internalization through RME. Hence, endocytosis of NPs depends on the size of the NPs and the receptor diffusion mechanism on the cell membrane. When the NPs are small, more energy is needed for membrane wrapping and clustering of NPs at the membrane to generate enough driving force for internalization. When the NPs are much bigger, they consume more receptors and there will be areas where not many receptors are available for NP internalization. Hence, there is an optimum size of 50 nm in the size range of 10-100 nm. These results are in agreement with the experiments carried out *in vitro* for as made or protein coated GNPs at monolayer cell level. However, our recent work with multilayer tissue-like cell models shows that smaller NPs are better at tumor tissue penetration than 50 nm GNPs. However, these NPs need to be functionalized with PEG to prevent their removal by the immune system during *in vivo* experiments. One of the drawbacks of having PEG on the NP surface is the reduction in uptake as shown in **Figure 4**[23, 29]. Hence, our first goal was to improve uptake of PEGylated NPs and to explore whether there is an optimum size.

We used a peptide (Arg-Gly-Asp, RGD) containing integrin binding peptide to increase the uptake of PEG-coated NPs [35]. In this study, we used 14 and 50 nm GNPs to investigate the effect of RGD peptides on the uptake of PEG-coated NPs, since 50 nm was better at a single cell level while smaller ones were better at tissue level. Introduction of the RGD peptide along with PEG enhanced the uptake of smaller NPs, but not the larger ones. The smaller NPs conjugated with PEG and RGD showed a three-fold increase in uptake as compared to PEG-coated NPs. We believe that the higher curvature of small NPs opens up space for RGD peptides to connect with the surface receptors on the cell membrane while these peptides can be hidden between PEG molecules on larger NPs due to lower surface curvature as explained in the schematic in **Figure 4**. Based on this, it is clear that smaller NPs coated with PEG and RGD peptides have a higher uptake as compared to 50 nm GNPs. One of the positives of this outcome is that smaller NPs penetrate tumor tissue better. This gives us the opportunity to use these smaller GNPs in applications such as radiation therapy.

The past decade has seen a dramatic increase in interest in the use of GNPs as radiation sensitizers for radiotherapy. This interest was initially driven by their strong absorption of ionizing radiation and the resulting ability to increase dose deposited within target tumor volume. Previous studies *in vitro* showed that radiosensitization correlated with the average number of gold nanoparticles internalized per cell[26]. Our data showed that cells internalized with citrate-capped GNPs of size 50 nm had higher cell death as compared to ones with smaller NPs (see **Figure 5**). Previous *in vivo* work has shown that nanoparticles of these dimensions can be effectively targeted to tumors by taking advantage of the enhanced permeation and retention effect[36], suggesting that the approach could allow for an increase in the tumoricidal effects while moderating toxicity to normal tissues. However, NPs need to be PEGylated for their applications *in vivo*. We noticed that PEGylated NPs have a very low uptake resulting in less radiation damage to tumor cells as shown in **Figure 5**. However, we were able to enhance cell death by a factor of four for smaller NPs once they were functionalized with a PEG-RGD combination. This is a very significant achievement since this study was conducted at clinically relevant 6 MV energies.

Given the novelty and significance of our results, we performed independent verification using enhancement of DNA DSBs in cells 24 h after irradiation. Exposure to ionizing radiation results in the production of a variety of DNA damage including single-strand breaks (SSBs), DSBs, DNA-base alterations, and DNADNA or DNA-protein crosslinks[37]. DSBs are the most lethal, and in this study we examined the protein 53BP1, which is associated with the sites of DSBs[38]. **Figures 5** and **7** show the extent to which DSBs for cells with internalized nanoparticles irradiated with 6 MV X rays. The quantification of DSBs using foci at 24 h provided a measure of the DSBs remaining after the treatment. Cells treated with PEG-RGD conjugated NPs showed an increase in DSBs in comparison to the ones internalized with PEG conjugated GNPs. These results are consistent with the cell damage data derived from the clonogenic assay as shown in **Figure 5**. Furthermore, we were able to map the DNA DSBs and the NPs localized within the cells as shown in **Figure 7**. It shows that cells treated with PEG-RGD coated NPs had more NPs and DNA DSBs than the cells treated with PEG coated GNPs. This is the first time that a correlation between DNA DSBs and number of GNPs localized within cells was shown using the technique of dark field imaging.

4. Conclusions

Engineering optimal GNPs for radiosensitization requires a thorough understanding of the physicochemical interactions of synthetic nanoparticles with biological systems. Based on our previous work and current study, it is evident that the optimum NP size can vary between monolayer level and multilayer tissue-like models based on their physicochemical properties. For example, when NPs are citrate capped, 50 nm ones are better at monolayer while smaller ones are better at tissue level. PEGylation of NPs along with RGD peptide resulted in a very different optimum size for cell uptake. Smaller NPs showed a higher uptake as compared to larger 50 nm GNPs. This is a positive result since smaller NPs penetrate better in tissue like materials. PEGylation of NPs allows them to stay in the blood and reach the tumor. Once they are within the tissue, their smaller size would help them penetrate the tumor tissue. The RGD peptide on these NPs will allow for their internalization into tumor cells effectively. Our radiation therapy experiments showed that cells treated with smaller NPs functionalized with RGD and PEG showed the highest cell death and DNA DSBs as compared to cells treated with GNPs functionalized with PEG alone. Over the past decade, there has been a great interest in using nanotechnology for cancer therapy. This work suggests that gold nanoparticles could be combined with radiation therapy for an increased therapeutic effect. It has been demonstrated that the addition of GNPs to cisplatin and other platinum agents enhanced radiation damage [39]. Hence, GNPs in combination with radiation and chemotherapeutic drugs provide interesting avenues to further improve the treatment of cancer.

5. Acknowledgements

The authors would like to acknowledge the Natural Sciences and Engineering Research Council of Canada (NSERC), Canadian Foundation for Innovation (CFI), and Keenen Research Center for their support. The authors would also like to acknowledge Dr. Richard P. Hill, Dr. R.G. Bristow, and Ms. R. Kumareswarren for their support.

6. References

1. K. Li, Z. Zhang, L. Zheng, H. Liu, W. Wei, Z. Li, Z. He, A. C. Larson and G. Zhang, *Nanomedicine*, 2015, 2185-2197.
2. B. B. Azad, S. R. Banerjee, M. Pullambhatla, S. Lacerda, C. A. Foss, Y. Wang, O. Ivkov and M. G. Pomper, *Nanoscale*, 2015, **7**, 4432-4442.
3. C. Cruje and B. D. Chithrani, *Journal of Nanoscience and Technology*, 2015, **15**, 2125-2131.
4. Q. Chen, H. Wang, H. Liu, S. Wen, H. Peng, M. Mingwu Shen, a. uixiang Zhang and X. Shi, *Analytical Chemistry*, 2015, **87**, 3949–3956.
5. S. D. Perrault, C. Walkey, T. Jennings, H. C. Fischer and W. C. W. Chan, *Nano Lett.*, 2009, **9**, 1909-1915.
6. Y. Ding, Y. Y. Zhou, H. Chen, D. D. Geng, J. Hong, W. B. Schen, T. J. Hang and C. Zhang, *Biomaterials*, 2013, **34**, 10217-10227.
7. S. D. Li and L. S. Huang, *J Control Release*, 2010, **145**, 178-181.
8. N. Niladri Chattopadhyay, Z. Zhongli Cai, J.-P. Jean-Philippe Pignol, B. Brian Keller, E. Eli Lechtman, R. Reina Bendayan and R. M. Reilly, *Mol Pharm.*, 2010, **7**, 2194–2206.
9. X. D. Zhang, D. Wu, P. X. Liu, N. Yang, B. Zhao, H. Zhang, Y.M. Sun, L. N. Zhang and F. Y. Fan, *Int J Namomed*, 2011, **6**, 2071-2081.
10. Y. Akiyama, I. T. Mor, Y. Katayama and T. Niidome, *J Control Release*, 2009, **139**, 81-84.
11. W. S. Cho, M. Cho, J. Jeong, M. Choi, B. S. Han, H. S. Shin, B. H. Hong, B. H. Chung, J. Jeong and M. H. Cho, *Toxicol Appl Pharmacol* 2010, **245**, 116-123.
12. T. Maldiney, C. Richard, J. Seguin, N. Wattier, M. Bessodes and D. Scherman, *ACS Nano*, 2011, **5**, 854-862.

13. R. Dharmatti, C. Phadke, A. Mewada, S. Pandey, G. Oza, C. Sharon and M. Sharon, *Journal of Nanomedicine Research*, 2014, **1**, 1-7.
14. G. Y. Lee, W. P. Qian, L. Wang, Y. A. Wang, C. A. Staley, M. Satpathy, S. Nie, H. Mao and L. Yang, *ACS nano*, 2013, **7**, 2078-2089.
15. H.-Q. Yin, F.-L. Bi and F. Gan, *Bioconjugate chemistry*, 2015, **26**, 243–249.
16. T. Zhan, P. Li, S. Bi, B. Dong, H. Song, H. Ren and I. Wang, *Journal of nanoscience and nanotechnology*, 2012, **12**, 7198-7205.
17. J. Lipka, M. Semmler-Behnke, R. A. Sperling, A. Wenk, S. Takenaka, C. Schleh, T. Kissel, W. J. Parak and W. G. Kreyling, *Biomaterials,*, 2010, **31**, 6574-6581.
18. A. Arnida, M. M. Janat-Amsbury, A. Ray, C. M. Peterson and H. Ghandehari, *Eur J Pharm Biopharm*, 2011, **77**, 417-423.
19. T. A. Larson, P. P. Joshi and K. Sokolov, *ACS Nano*, 2012, **6**, 9182–9190.
20. C. D. Walkey, J. B. Olsen, H. Guo, A. Emili and W. C. Chan, *J Am Chem Soc*, 2012, **134**, 2139-2147.
21. A. N. Gordon, C. O. Granai, P. G. Rose, J. Hainsworth, A. Lopez, C. Weissman, R. Rosales and T. Sharpington, *J Clin Oncol*, 2000, **18**, 3093–3100.
22. R. A. Petros and J. M. DeSimone, *Nat Rev Drug Discov*, 2010, **9**, 615-627.
23. P. Nativo, I. A. Prior and M. Brust, *ACS Nano*, 2008, **2**, 1639-1644.
24. N. Kohler, C. C. Sun, J. Wang and M. Zhang, *Langmuir*, 2005, **21**, 8858-8864.
25. P. Podsiadlo, V. A. Sinani, J. H. Bahng, N. W. Kam, J. Lee and N. A. Kotov, *Langmuir* 2008, **24**, 568-574
26. B. D. Chithrani, S. Jelveh, F. Jalali, M. Van Prooijen, C. Allen, R. G. Bristow, R. P. Hill and D. A. Jaffray, *Radiat. Res.*, 2010, **173**, 719-728.
27. S. H. Cho, *Phys. Med. Biol.*, 2005, **50**, N163-N173.
28. Q. Dai, C. Walkey and W. C. Chan, *Angew Chem Int Ed Engl*, 2014, **53**, 5093-5096.
29. Y. Liu, M. K. Shipton, J. Ryan, E. D. Kaufman, S. Franzen and D. L. Feldheim, *Anal Chem* 2007, **79**, 2221-2229.
30. B. D. Chithrani, A. A. Ghazani and W. C. W. Chan, *Nano Lett*, 2006, **6**, 662-668.
31. C. cruje and B. D. Chithrani, *Nanomed Res.*, 2015, **1**, 1-6.
32. M. Neshatian, S. Chung, D. Yohan, C. Yang and D. B. Chithrani, *J Biomed Nanotechnol* 2015, **11**, 1162-1172.
33. D. Yohan, C. Charmainne, X. Lu and B. D. Chithrani, *Nano-Micro Lett*, 2015, **Accepted**.
34. J. P. Banath and P. L. Olive, *Cancer Res.*, 2003, **63**, 4347–4350.
35. L. Kong, C. S. Alves, W. Hou, J. Qiu, H. Möhwald, H. Tomás and X. Shi, *ACS Appl Mater Interfaces*, 2015, **7**, 4833-4843.
36. H. F. Dvorak, J. A. Nagy, J. T. Dvorak and A. M. Dvorak, *Am. J. Pathol*, 1988, **133**, 95–109.
37. T. Helleday, E. Petermann, C. Lundin, B. Hodgson and R. A. Sharma, *Nat. Rev. Cancer*, 2008, **8**, 193–204.
38. R. G. Bristow and R. P. Hill, *Nat. Rev. Cancer*, 2008, **8**, 180–192.
39. Y. Zheng and L. Sanche, *Radiat. Res.*, 2009, **172**, 114-119.

Optimization of PEG Coated Nanoscale Gold Particles for Enhanced Radiation Therapy

Graphical abstract

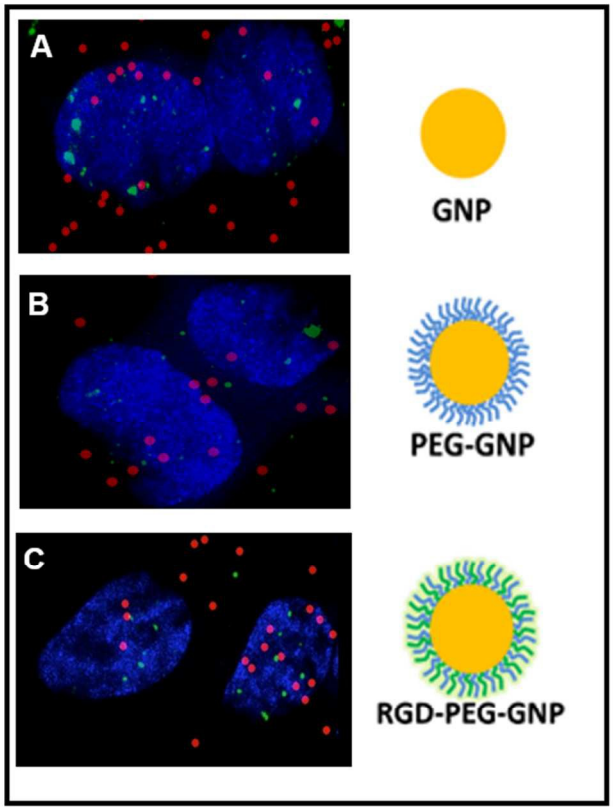

Table of contents Figure. Enhanced sensitization by targeted GNPs over non-targeted at clinically relevant MeV energies. (A-C) Mapping of GNP distribution and DNA DSBs within tumor cells after a radiation treatment with clinically relevant MeV energies. Uptake of PEGylated NPs could be improved after co-functionalization with a peptide containing RGD domain. More DNA DSBs can be seen in cells targeted with RGD-PEG-GNPs vs PEG-GNPs. This study will accelerate clinical use of GNPs in future cancer therapy.